MITIGATING TSUNAMI DAMAGE BY PROMOTING GROUND EROSION

Takegawa, Naoki

Sawada, Yutaka

Kawabata, Toshinori

Journal of Earthquake and Tsunami

MITIGATING TSUNAMI DAMAGE BY PROMOTING GROUND EROSION

Naoki Takegawa (First Author)

INSTITUTION 1

National Metrology Institute of Japan, National Institute of Advanced Industrial Science and Technology
1–1–1, Umezono, Tsukuba, Ibaraki, 305–8563, Japan
takegawa-naoki@aist.go.jp, ORCID iD: 0000-0002-6814-9827

INSTITUTION 2

Graduate School of Agricultural Science, Kobe University
1–1 Rokkodai, Nada, Kobe, Hyogo, 657–8501, Japan

Yutaka SAWADA (Corresponding Author)

Graduate School of Agricultural Science, Kobe University
1–1 Rokkodai, Nada, Kobe, Hyogo, 657–8501, Japan
sawa@harbor.kobe-u.ac.jp, ORCID iD: 0000-0001-5517-3345

Toshinori KAWABATA

Graduate School of Agricultural Science, Kobe University
1–1 Rokkodai, Nada, Kobe, Hyogo, 657–8501, Japan
kawabata@kobe-u.ac.jp

Received (Day Month Year)
Revised (Day Month Year)
Accepted (Day Month Year)

To reduce the damage caused when a tsunami overflows coastal dikes, this study performs hydraulic experiments and numerical simulations and proposes a new method for slowing the tsunami by intentionally eroding parts of the ground. The effectiveness of the proposed method is assessed, velocity-reduction mechanism is clarified, and reduced tsunami velocity is predicted. Using crushed expanded polystyrene as the ground material, vertical erosion is enhanced and a large depression is formed that changes the flow from supercritical to subcritical, thereby decelerating it. Assuming a constant tsunami overflow rate, the tsunami velocity after deceleration can be predicted with ~20% uncertainty.

Keywords: Tsunami disaster mitigation; velocity reduction; erosion; hydraulic jump; hydraulic experiment; numerical simulation.

1. Introduction

In Japan, the construction of coastal dikes has been progressing rapidly to recover from the tsunami damage caused by the Great East Japan Earthquake of 2011 and to prepare for a huge earthquake that is likely to occur in the near future. From the viewpoint of construction costs and environmental conservation, the basic idea is to allow the overflow of a large-scale tsunami, and there are two important points as shown in Fig. 1, namely (i) preventing the tsunami overflow from breaching the dike and (ii) slowing the tsunami as much as possible after overflow to give enough time for evacuation and reduce structural damage. In the case of (i), field surveys and model experiments have shown that one of the main factors affecting stability is the tsunami overflow scouring the ground on the landward side of coastal facilities [Kato *et al.* 2012; Kawasaki 2012; Mikami *et al.* 2012; Tokida and Tanimoto 2014]. Iiboshi *et al.* [2015], Mitobe *et al.* [2014], and Takegawa *et al.* [2020a, b] have studied scour countermeasures for the ground on the landward side of coastal dikes. Because a tsunami due to a huge earthquake continues to be a concern, knowledge about scour countermeasures is extremely important for realizing retentive coastal dikes. Regarding (ii), Tanimoto *et al.* [2012], Tanimoto and Tokida [2012] and Tokida and Tanimoto [2014] reported that although the breaching of a coastal dike is due to the scour hole immediately behind it, that scour hole also acts to reduce the tsunami velocity. Also, Kiri *et al.* [2015] proposed tsunami deceleration by excavating in advance the ground on the landward side of a coastal dike; they verified experimentally the effectiveness of doing so, and their experimental results showed that the horizontal velocity was reduced by as much as approximately 30%. However, Kiri *et al.* [2015] concluded that such velocity-reduction work must also protect people from falling and consider the stability of the coastal dike. Also, regarding land use, it is undesirable to have such permanent measures against a tsunami attack with a low probability of occurring.

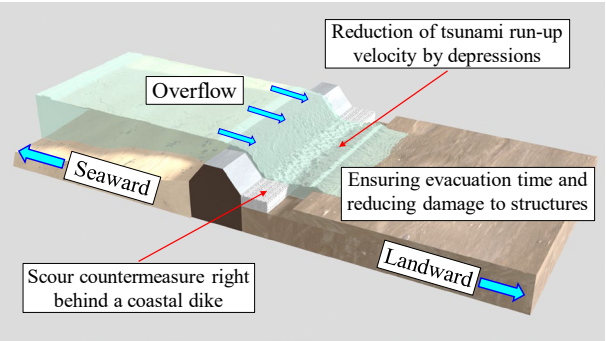

Fig. 1 Reduction of the scour on landside ground behind coastal dikes and tsunami run-up velocity for mitigation of tsunami damage.

To overcome the aforementioned problems, a new method is proposed herein that involves using the erosion effect of the tsunami itself to do the velocity-reduction work. In this method, part of the ground is replaced in advance with a lightweight material to

promote intentional ground erosion during a tsunami overflow. Consequently, the land can be used effectively at all times, and fall-prevention measures are unnecessary. In the present study, hydraulic model experiments and numerical simulations were performed to assess the effectiveness of the proposed method and the mechanism for velocity reduction. Also, the overflow rate and the dike height are used to estimate the reduced tsunami velocity due to the proposed method.

2. Reduced horizontal velocity by promoting ground erosion

2.1. *Outline of experiments*

To promote ground erosion during a tsunami overflow, we focus on the density, particle size, and submerged specific gravity (SSG) of the ground material, and we conducted hydraulic experiments to investigate their effects. Figure 2 shows the acrylic channel (length: 2000 mm; width: 100 mm) that was used in the experiments. A flow rate Q of 2.0 L/s was generated in the channel using a pump, flow control valve, and flow meter (manufacturer: TOKYO KEISO CO., LTD., model number: O-180-SC-032-2F, measurement accuracy: ±0.067 L/s). The ground and water surface profiles were recorded as images using a video camera, and the coordinates of the surface profiles were calculated by counting the number of pixels in the obtained images. The experimental cases listed in Table 1 were conducted to assess how the ground conditions affect the erosion. The physical properties of the ground material are given in Table 2. In cases 1–4, the Froude number ($v/\sqrt{gh}$) upstream of the ground was approximately 0.56; in cases 5 and 6, a weir was installed to increase the Froude number to approximately 2.0; in cases 4 and 6, a designated volume (100 mm × 100 mm × 100 mm) of the ground was backfilled with crushed expanded polystyrene (EPS). It is important to note that the weir in cases 5 and 6 (Fig. 2(c)) was installed to increase the horizontal velocity (i.e., the Froude number) and is not treated as a dike model. In other words, we do not assume a scale in Sec. 2. Conversely, in Sec. 4, the weir is treated as a dike model to estimate the reduced tsunami velocity because Sec. 4 focuses only on the flow of water, and the similarity law can be applied. Because the horizontal velocity in Sec. 2 is likely to be smaller than the real scale, we verify whether the erosion occurs sufficiently under the present experimental conditions in terms of the Shields number.

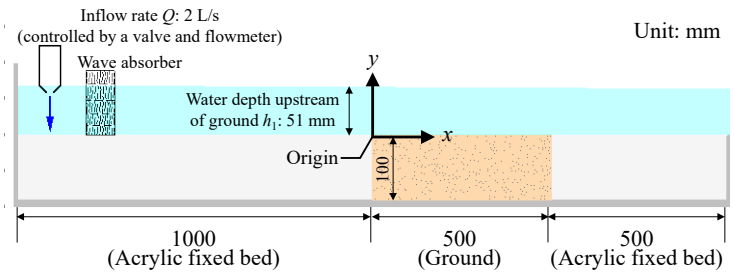

(a) Front view of cases 1–4.

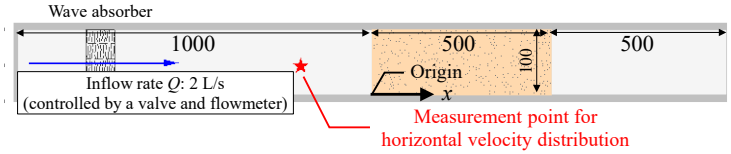

(b) Top view of cases 1–4.

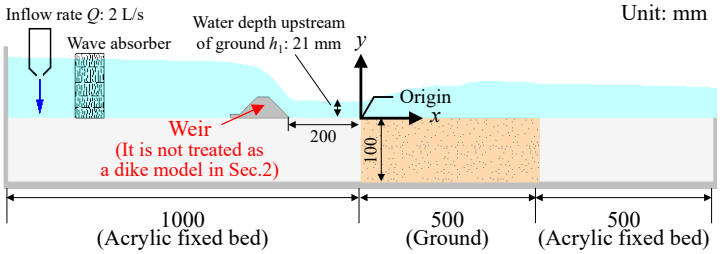

(c) Front view of cases 5 and 6.

Fig. 2 Experimental apparatus used in Sec. 2. The measurement point for the horizontal velocity is shown in Fig. 2 (b). The weir shown in Fig. 2 (c) is not treated as a dike model in Sec. 2.

Table 1 Experimental cases in Sec. 2.

	Ground material	Relative density *Dr*	Water depth upstream of ground h_1	Velocity upstream of ground v_1	Froude Number *Fr*
Case1	Silica-L	90%	51 mm	390 mm/s	0.56
Case2	Silica-L	15%	51 mm	390 mm/s	0.56
Case3	Silica-S	90%	51 mm	390 mm/s	0.56
Case4	Silica-L with crushed EPS	90%	51 mm	390 mm/s	0.56
Case5	Silica-L	90%	21 mm	940 mm/s	2.0
Case6	Silica-L with crushed EPS	90%	21 mm	940 mm/s	2.0

Table 2 Physical properties of the ground material.

	Silica-L	Silica-S	Crushed EPS
Density of sand particle ρ_s (g/cm^3)	2.63	2.63	0.070
Maximum dry density ρ_{max} (g/cm^3)	1.59	1.57	0.068
Minimum dry density ρ_{min} (g/cm^3)	1.27	1.15	0.054
Median particle diameter D_{50} (mm)	0.21	0.11	3.40
Geometric standard deviation σ_g	1.39	1.49	1.26

The relationship between the experimental conditions and ground erosion was assessed for subcritical flow (cases 1–4). Figure 3 shows the horizontal velocity

distribution on the fixed bed measured using a pitot tube (manufacturer: OKANO WORKS, LTD., model number: LK-0, measurement accuracy: ±5%). The locations of the fixed bed and measurement point are shown in Fig. 2(a) and (b). Here, the friction velocity u^* is calculated from the horizontal velocity distribution and the Prandtl–Kármán law, namely,

$$\frac{u}{u^*} = \frac{1}{\kappa}\ln\frac{u^* y}{\nu} + C, \tag{1}$$

$$u = \frac{u^*}{\kappa}\ln y + \left(\frac{u^*}{\kappa}\ln\frac{u^*}{\nu} + Cu^*\right), \tag{2}$$

where u is the horizontal velocity, κ is the Kármán constant, ν is the kinematic viscosity, y is the height from the channel bottom, and C is an experimental constant. Assuming κ = 0.4, the friction velocity u^* is 150 mm/s based on the slope (u^*/κ) of the plots shown in Fig 3. Note that because it is difficult to measure the velocity distribution on the ground owing to the progress of erosion, the friction velocity at the fixed bed is calculated and the relationship between the experimental conditions and ground erosion is discussed based on this value. The Shields number τ_* for Silica-L (Table 2) is approximately 7.0 according to

$$\tau_* = \frac{u_*^2}{sgd}, \tag{3}$$

where s is the SSG of the ground material, g is the gravitational acceleration, and d is the median particle diameter of Silica-L. The critical Shields number τ_c agrees well with that calculated using the equation due to Iwagaki [1956], namely

$$\tau_c = \frac{8.41}{sgd^{\frac{21}{32}}}\ (0.065\ mm < d < 0.565\ mm). \tag{4}$$

Using the median particle diameter of Silica-L, the critical Shields number τ_c is approximately 0.07, and therefore the Shields number (i.e., τ_* = 7.0) in the present experiments is large enough to ensure erosion of the sand particles.

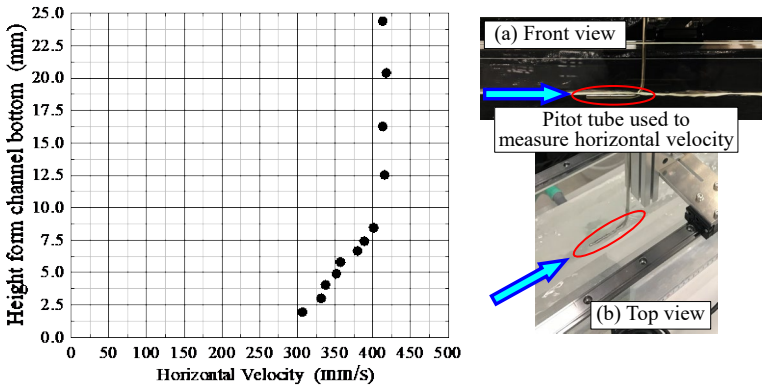

Fig. 3 Horizontal velocity distribution on the fixed bed measured using a pitot tube.

2.2. *Experimental results on promoting ground erosion (cases 1–4, Fr = 0.56)*

For cases 1–3, Figure 4 shows the ground profiles in the front of the acrylic channel. The upstream end of the ground at the initial surface height is treated as the origin, as shown in Fig. 2. As the experiment progressed, the horizontal flow crashed with the downstream fixed bed and erosion locally developed after x = 400 mm. Therefore, this study focuses on experimental results of up to x = 400 mm. Comparing case 1 (ground material: Silica-L; relative density: 90%) and case 2 (ground material: Silica-L; relative density: 15%) 30 min after the start of the experiment, although the ground profiles differ slightly until approximately x = 100 mm, they agree thereafter. This means that the ground density has little influence on the erosion due to horizontal flow. The surface erosion does not depend on the ground density, and the dominant relationship is between the resistance of a surface particle and the fluid force. Comparing case 1 with case 3 (ground material: Silica-S; relative density: 90%), because the Shields number increases with decreasing particle diameter, erosion is expected in case 3. However, the development of erosion is actually confirmed in case 1, for which the particle diameter is larger. Although the reason for this is unclear, it is thought that an effect other than the weight of the particles offered resistance to the fluid force. Figure 5 shows the relationship between the velocity and erosion, transport, and sedimentation [Hjulstrom, 1935]. When the particle diameter is less than 0.1 mm, the critical velocity increases with decreasing diameter. The median particle diameter D_{50} of Silica-S is 0.11 mm, which is located at the border where the critical velocity increases with decreasing diameter. Therefore, there is a possibility that erosion did not progress in case 3. Although the erosion profiles of the three cases differ slightly, the point to note here is that the depth of the depressions caused by the erosion is approximately 20 mm at the most in Fig. 4, indicating that the depressions are extremely small. As described in Sub-sec. 2.1, the conditions for erosion of sand particles in these experiments are deemed to be satisfied sufficiently. Therefore, it is clear that vertical erosion does not always develop even under hydraulic conditions exceeding the critical

Shields number. This is an important finding in the context of reducing the tsunami velocity by changing the ground profile.

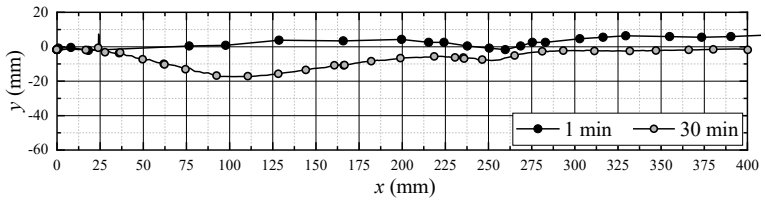

(a) Case 1 (Silica-L, *Dr* = 90%).

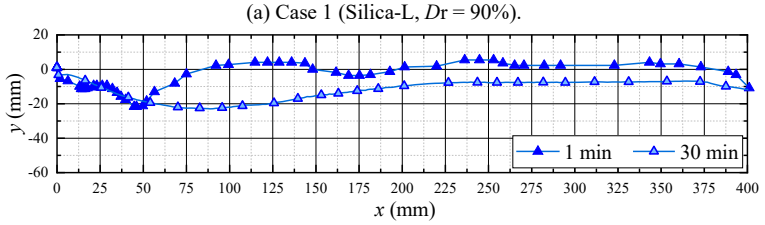

(b) Case 2 (Silica-L, *Dr* = 15%).

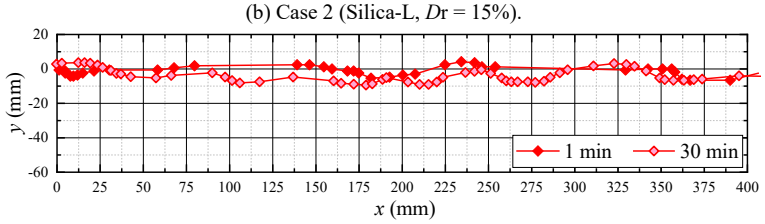

(c) Case 3 (Silica-S, *Dr* = 90%).

Fig. 4 Ground profile at 1 min and 30 min. Ground profile was recorded as images using a video camera, and coordinates were calculated by counting the number of pixels in the obtained images.

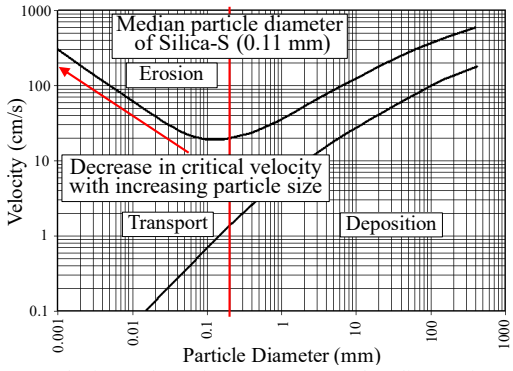

Fig. 5 Relationship between velocity and erosion, transport, and sedimentation (modified from Hjulstrom [1935]).

In the present study, we focused on the SSG *s*, which is included in the Shields number, as a different approach to promoting vertical erosion. Crushed EPS has a negative SSG because the particle density ρ_s is only 0.07 g/cm^3. Figure 6 shows the transition of the ground profile for case 4 (crushed EPS). There is no change in the

backfill area using crushed EPS until 5 s. Then, 6 s after the start of the experiment (Fig. 6(b)), it is confirmed that the crushed EPS at the top of the backfill area flows downstream because of buoyancy. Then, 8 s after the start of the experiment (Fig. 6(c)), all of the crushed EPS is lifted upward and almost all of it is transported (Fig. 6(d)). In this experiment, large-scale vertical erosion was achieved successfully in a very short time, and regarding promoting vertical erosion, it can be concluded that reducing the SSG is effective.

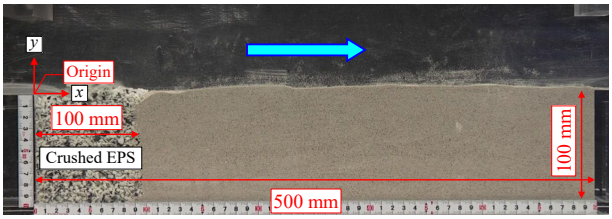

(a) 0 s.

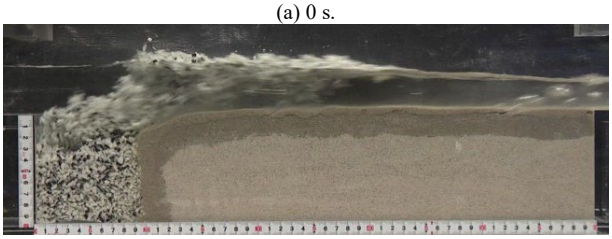

(b) 6 s.

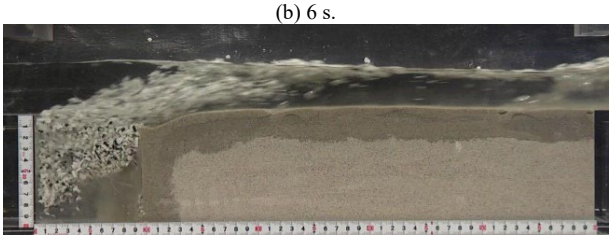

(c) 8 s.

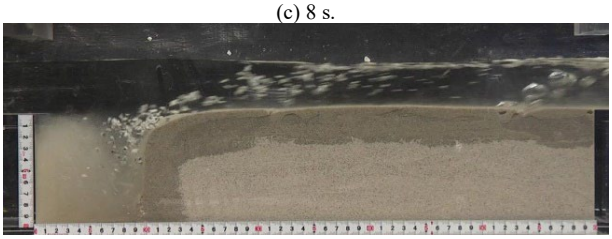

(d) 10 s.

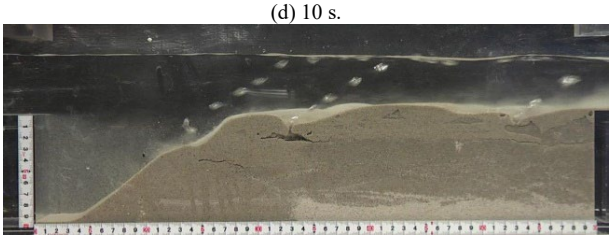

(e) 60 s.

Fig. 6 Transition of the ground profile for case 4 (crushed EPS).

2.3. *Experimental results on relationship between ground profile and reduction of horizontal velocity (cases 1–6)*

In this subsection, we clarify how the ground profile affects the horizontal velocity. Figure 7 shows the water and ground surface profiles for cases 1–4 30 s after the start of the experiment. In case 4, although the crushed EPS leaves a large depression, the water depth (velocity) at each location is almost the same as that in cases 1–3. This result shows that when the flow is subcritical, large energy loss may not occur even if the depression is provided. Figure 8 shows the relationship between the specific energy E and the water depth h in this experiment using

$$E = \frac{q^2}{2gh^2} + h, \tag{5}$$

where q is the flow rate per unit width. In Fig. 8, the water depth decreases and the velocity increases with energy loss (decrease in specific energy) for subcritical flow with constant flow rate. Therefore, under those conditions, it is considered that the velocity cannot be reduced even when a large depression forms.

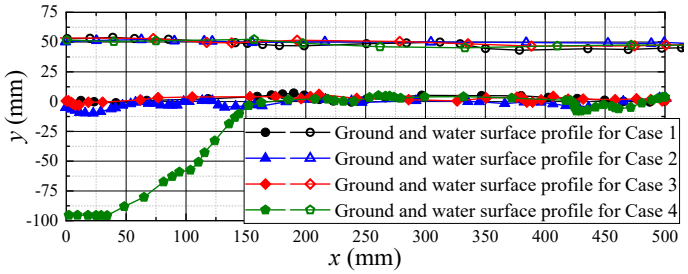

Fig. 7 Water and ground surface profiles for cases 1–4, 30 s after the start of the experiment.

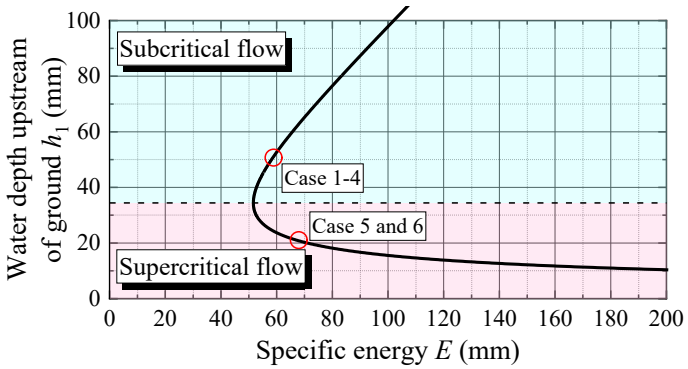

Fig. 8 Relationship between specific energy E and water depth h in this experiment.

Figure 9 shows the changes in the horizontal velocity in cases 5 and 6 (Fr = 2.0) at the origin. The velocity was calculated by dividing the flow rate (2.0 L/s) by the water depth determined form the images. The formation of the depression changes the flow from supercritical to subcritical (hydraulic jump), and the velocity decreases. After 1 min, the velocity is almost the same in cases 5 and 6 and is reduced by approximately 60% from the initial condition. In other words, using the depression to reduce the tsunami velocity is effective when the flow is supercritical. Although decreased velocity is confirmed even in case 5 (ground material: Silica-L; relative density: 90%) where no erosion is promoted, the use of the method remains necessary because it is effective for the ground where erosion is less likely to occur than Silica-L and the extent to which the erosion is promoted can be grasped in advance.

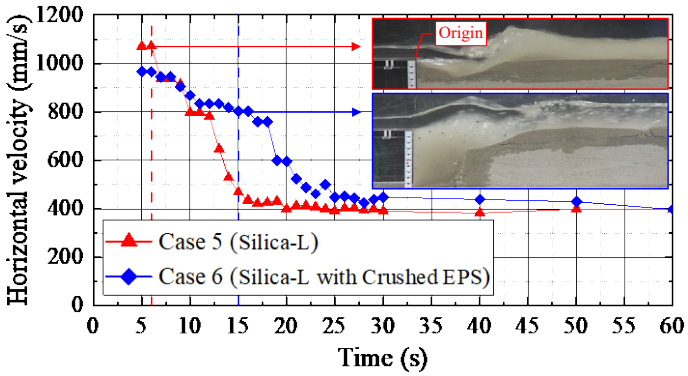

Fig. 9 Changes in the horizontal velocity in cases 5 and 6 (Fr = 2.0) at the origin. The horizontal velocity was calculated by dividing the flow rate (2.0 L/s) by the water depth determined form images.

3. Mechanism for reduced horizontal velocity due to ground depression on landward side of coastal dike

3.1. *Outline of numerical simulation*

To investigate the mechanism for a hydraulic jump caused by a ground depression on the landward side of a coastal dike, we performed numerical simulations using OpenFOAM [2019] Foundation. The simulations are the two-phase flow (water and air) of an isothermal, incompressible, and immiscible fluid. The finite volume method is used to solve the governing equations (the continuity and momentum equations) given by

$$\nabla \cdot \boldsymbol{U} = 0, \tag{6}$$

$$\frac{\partial \rho \boldsymbol{U}}{\partial t} + \nabla \cdot (\rho \boldsymbol{U}\boldsymbol{U}) = -\nabla p^* + \nabla \boldsymbol{\tau} + \rho \boldsymbol{g} + f_s, \tag{7}$$

where $\boldsymbol{U}$ is the velocity vector, ρ is the density, p^* is the pressure minus the hydrostatic potential, $\boldsymbol{\tau}$ is the viscous stress tensor, $\boldsymbol{g}$ is the gravitational acceleration, and f_s represents the surface tension. The pressure–velocity coupling is handled using the

PIMPLE (Pressure-Implicit Method for Pressure-Linked Equations) algorithm. The VOF (Volume of Fluid) method is used to track the air–water interface, and the advection equation is given by

$$\frac{\partial \alpha}{\partial t} + \nabla \cdot \boldsymbol{U}\alpha + \nabla \cdot U_c \alpha(1-\alpha) = 0, \tag{8}$$

where α is the volume fraction, which is assigned value 0 in air and 1 in water, and U_c is the relative velocity vectors of the air and water phases. Figure 10 and Table 3 describe the simulation region and conditions. The ground depression was reproduced by providing the steps. Similar to the experimental cases 5 and 6 in Sec. 2, the flow rate Q was 2.0 L/s and the water depth upstream of step h_1 and Froude number Fr were 21 mm and 2.0, respectively. From the previous experiment, it was found that the hydraulic jump occurred at a step height of 5.3 mm ($s/h_1 = 0.25$) or more when $Q = 2.0$ L/s; this height is defined as the critical step height s_c. In the numerical simulations, two values of the step height s were set, namely, one less than the critical step height (i.e., $s = 3.5$ mm) and one greater than the critical step height (i.e., $s = 10$ mm).

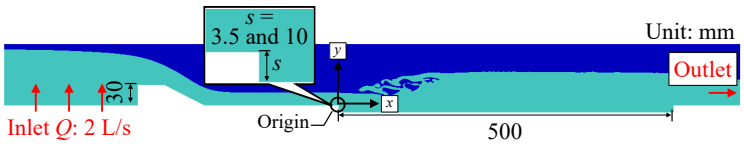

Fig. 10 Simulation region

Table 3 Simulation conditions

Flow rate Q (L/s)	2.0
Water depth upstream of ground h_1 (mm)	21
Froude Number Fr	2.0
Step height s (mm)	3.5, 10.0
Grid spacing (mm)	0.5–1.0
Total number of cells	s = 3.5 mm: 95900 s = 10.0 mm: 102400
Boundary condition for velocity	Wall: no-slip Top: pressureInletOutletVelocity Left: flowRateInletVelocity (2.0 L/s) Outlet: inletOutlet
Solver	interFoam
Turbulence model	k-ε model

3.2. *Results of numerical simulation*

Figure 11 shows water surface profiles from the experiments and simulations after the flow had stabilized sufficiently. The numerical results agree well with the experimental ones for both $s < s_c$ and $s > s_c$, thereby validating the numerical analysis.

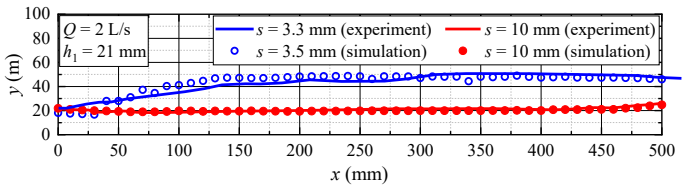

Fig. 11 Water surface profiles for the experiment and simulation.

Figure 12 shows the pressure distribution at s = 3.5 and 10 mm. For s = 3.5 mm, no hydraulic jump occurs over the entire channel, and the pressure is calculated under stable flow conditions. For s = 10 mm, the pressure distribution when the flow reaches the step on the downstream side is extracted because the flow state just before the hydraulic jump occurs is deemed important. The blue plot in Fig. 12 shows the pressure difference from the point 1 mm downstream (i.e., pressure gradient) given by

$$\frac{\partial P_x}{\partial x} = \frac{P_{x+1} - P_x}{\Delta x\ (= 1\ mm)}. \tag{9}$$

Positive and negative values in the blue plot indicate adverse and favorable pressure gradients, respectively. Unlike in the case of s = 3.5 mm, a large area of an adverse pressure gradient develops behind the step for s = 10 mm. From the contours for s = 10 mm, the pressure drops behind the step (x = 0–20 mm) and then increases at the bottom of the channel (x = 30–50 mm). It is thought that the flow became downward behind the step (x = 0–20 mm) because of the pressure drop and collided with the bottom of the channel, resulting in a large reverse pressure gradient. Moore and Morgan [1959], Rajaratnam and Ortiz [1977], Hager and Bretz [1986], and Ohtsu and Yasuda [1991] researched step flows in detail. In particular, Ohtsu and Yasuda [1991] noted that downward flow occurs when the flow at the step is supercritical at $s/h_1 < 0.5$–1.5, and the simulation results are consistent with that observation. In the case of the step on the downstream side, although the adverse pressure gradient is confirmed for both s = 10 mm and s = 3.5 mm, it is smaller than that when the step is on the upstream side. Therefore, having the step on the upstream side of the depression is important for generating an erosion-induced hydraulic jump. It is therefore necessary to provide a step height that is sufficient to generate a pressure drop and a downward flow behind the depression.

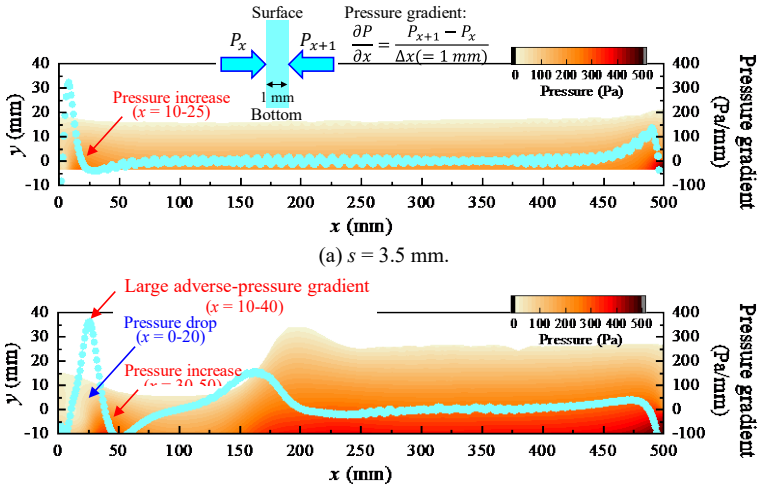

(a) s = 3.5 mm.

(b) s = 10.0 mm.

Fig. 12 Pressure distribution and gradient at s = 3.5 and 10 mm. The blue plot shows the pressure gradient.

4. Predicting tsunami velocity after dike overflow

From the perspective of reducing tsunami damage to both structures and people, it is important not only to reduce the tsunami velocity but also to predict that velocity, and numerical simulation is effective for the latter. However, such simulations require time and skill and are not practically possible for all coastal dikes. Therefore, it is extremely important to develop a predictive formula for the approximate velocity. We assume an overflow of a tsunami with a large wavelength at a constant flow rate, and we predict (i) the tsunami velocity on the ground on the landward side immediately behind a coastal dike and (ii) the velocity after the hydraulic jump caused by the depression (i.e., the tsunami run-up velocity). Figure 13 shows a diagram of the hydraulic experiments in Sec. 4. The step height was approximately 6 mm, and we used six flow rates, namely, 0.5, 0.7, 1.0, 1.3, 1.7, and 2.0 L/s. Unlike Sec. 2, Sec. 4 focuses only on the flow of water; hence, it is possible to apply the Froude similarity. Therefore, the weir shown in Fig. 13 is treated as a dike model in Sec. 4. For instance, for Q = 2.0 L/s, when the landward conditions (dike height H: 30 mm and velocity upstream of ground v_1: 940 mm/s) are increased by a factor of 400 based on the Froude similarity, the water depth H and velocity v_1 will be approximately 12.0 m and 18.8 m/s, respectively.

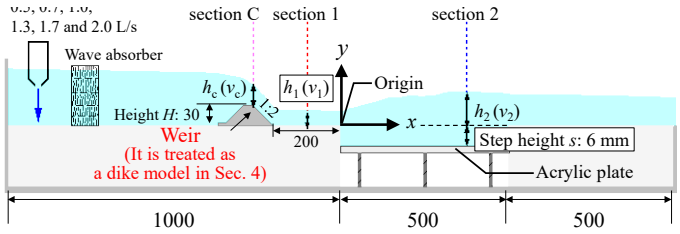

Fig. 13 Experimental apparatus used in Sec. 4.

When the overflow on the ground on the landward side of a coastal dike is supercritical, the water depth and velocity at a point on the top of the dike are equal to the critical water depth h_c and the critical velocity v_c, where the critical water depth h_c is given by

$$h_c = \sqrt[3]{\frac{q^2}{g}}. \tag{10}$$

Applying Bernoulli's equation to cross sections C and 1 in Fig. 13 yields

$$H + h_c + \frac{{v_c}^2}{2g} = h_1 + \frac{{v_1}^2}{2g}. \tag{11}$$

Then, the continuity equation

$$q = h_c v_c = h_1 v_1 \tag{12}$$

gives the cubic equation

$${h_1}^3 - \left(H + h_c + \frac{{v_c}^2}{2g}\right){h_1}^2 + \frac{{h_c}^2}{2g}{v_c}^2 = 0 \tag{13}$$

for the water depth h_1 on the ground immediately behind the coastal dike.

Equation (13) can be solved using the Cardano's method. The horizontal velocity v_1 can be obtained from the calculated water depth h_1, and the water depth h_2 after the hydraulic jump is given by

$$h_2 = -\frac{h_1}{2} + \sqrt{\frac{{h_1}^2}{4} + \frac{2q^2}{gh_1}}. \tag{14}$$

Note that Eq. (14) is for horizontal flow and is not strictly applicable when there are depressions and steps. However, Ohtsu and Yasuda [1991] reported that the flow

conditions approach those of a free jump in a horizontal channel for $s/h_1 \leq 0.5$–1.5. Therefore, the present study also predicts the water depth h_2 downstream of the hydraulic jump using Eq. (14).

Figure 14 compares the horizontal velocities v_1 and v_2 in terms of the experimental values and those predicted using Eq. (13) and (14). The red plot of predicted values of v_1 was calculated using Eq. (13), and the blue plot of predicted values of v_2 was calculated by substituting h_1 derived from Eq. (13) into Eq. (14). In other words, the post-deceleration velocity v_2 is predicted from only the overflow rate q and dike height H. The values of v_1 predicted by Eq. (13) are 20–40% larger than those measured experimentally, which is thought to be because Eq. (11) does not account for frictional effects. Because the predicted values of v_1 are larger than the experimental values, v_2 derived using v_1 is 10%–20% smaller than the experimental values. Although the post-deceleration tsunami run-up velocity v_2 is subject to an error of approximately 20%, the simple predictive method using only the overflow rate q and dike height H is considered to be extremely useful in practice because it would be handled easily by a wide range of engineers.

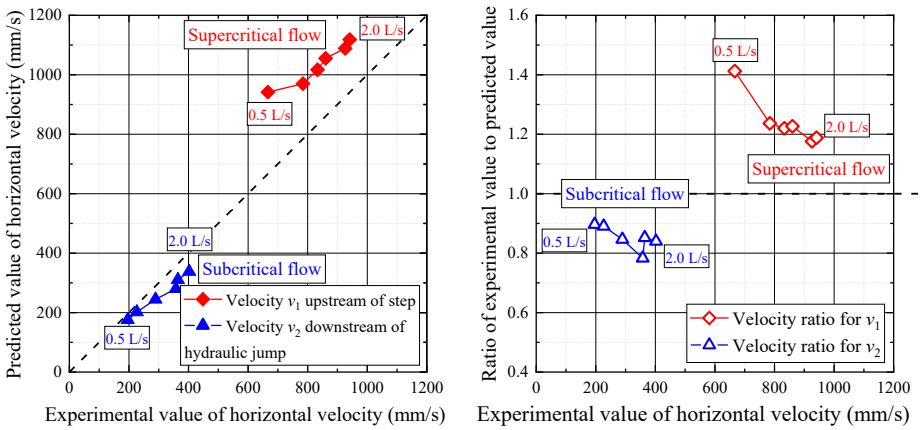

Fig. 14 Comparison of horizontal velocities of v_1 and v_2 between experimental and predicted values. The blue and red plots indicate the velocity upstream of step and velocity downstream of hydraulic jump, respectively. Six flow rates were tested, namely, 0.5, 0.7, 1.0, 1.3 1.7, and 2.0 L/s.

5. Summary

In this study, to reduce the damage caused by a tsunami overflowing coastal dikes, we devised a new method to slow the tsunami by intentionally allowing it to erode part of the ground. Furthermore, we (i) assessed the method's effectiveness, (ii) clarified the mechanism for the velocity reduction, and (iii) predicted the reduced tsunami velocity. The findings obtained are listed below.

1. Under hydraulic conditions exceeding the critical Shields number, there was hardly any vertical erosion in the experiments with different ground densities and particle sizes. When the crushed EPS with low SSG was used as the ground material, the

vertical erosion was greatly enhanced. From the perspective of promoting erosion, it is effective to reduce the SSG.

2. When the flow was subcritical with a constant flow rate, the same water surface profiles (velocity) were observed regardless of the ground surface profile. This result shows that the velocity cannot be reduced even if a depression is provided. When the flow was supercritical, the depression that formed changed the flow from supercritical to subcritical, and the flow velocity decreased. Thus, reducing the tsunami velocity by means of a depression is effective for supercritical flow.
3. Numerical simulations were performed on step flows to simulate a depression formed by erosion promotion. When a hydraulic jump occurred, the region of reduced pressure diverted the flow behind the step downward, whereupon the flow collided with the channel bottom and a large adverse pressure gradient arose. This gradient is considered to contribute to the occurrence of the hydraulic jump.
4. Assuming a tsunami overflow to be a constant flow rate, we predicted (i) the tsunami velocity on the ground on the landward side immediately behind the coastal dike and (ii) the velocity after the hydraulic jump caused by the depression (the tsunami run-up velocity). Comparing the predicted results with the present experimental results show that the post-deceleration tsunami run-up velocity v_2 can be predicted with an uncertainty of approximately 20%. The simple predictive method using only the overflow rate q and dike height H is considered to be extremely useful given that it would be handled easily by general engineers.

Acknowledgments

This work was supported by JSPS Grant-in-Aid for Challenging Research Exploratory under Grant [number 18K19248].

References

Hager, W., and Bretz, N. [1986] "Hydraulic jumps at positive and negative steps," *J. Hydraul. Res.* **24**(4), 237–253.

Hjulstrom, F. [1935] "Studies of the morphological activity of rivers as illustrated by the River Fyris," *Geol. Inst. Upsalsa* **25**, 221–527.

Iwagaki, Y. [1956] "Hydrodynamical study on critical tractive force," *Trans. Jpn. Soc. Civil Eng.* **41,** 1–21. (in Japanese)

Iiboshi, T., Maeno, S., Yosida, K., Takata, D. and Yamamura, A. [2015] "Effects of landward slope protection and toe protection work shape at coastal dikes on landward bed scouring caused by tsunami overflow," *Proc. of 36th Int. IAHR World Congress*, Hague, Netherlands, pp. 4103–4111.

Kato, F., Suwa, Y., Watanabe, K. and Hatogai, S. [2012] "Mechanisms of coastal dike failure induced by the Great East Japan Earthquake tsunami," *Proc. of 33rd Int. Conf. on Coastal Engineering*, Santander, Spain, doi.org/10.9753/icce.v33.structures.40.

Kawasaki, K. [2012] "Fundamental characteristics of tsunami and tsunami disaster due to the 2011 off the Pacific Coast of Tohoku Earthquake," *Jpn. Soc. Multiph. Flow* **26**(1), 11–18. (in Japanese)

Kiri, H., Nakaya, T., Azechi, I. and Matsushima, K. [2015] "Effect of the Tsunami Dissipation Facility that Modeled a Pool at the Toe of Back Slope of the Coastal Levees," *J. Jpn. Soc. Civ. Eng. Ser. B1* **71**(4), I_1369–I_1374. (in Japanese)

Mikami, T., Shibayama, T. and Esteban, M. [2012] "Field Survey of the 2011 Tohoku Earthquake and Tsunami in Miyagi and Fukushima Prefectures," *Coast. Eng. J.* **54**(1), 1–26.

Mitobe, Y., Adityawan, M.B., Tanaka, H., Kawahara, T., Kurosawa, T. and Otsushi, K. [2014] "Experiments on local scour behind coastal dikes induced by tsunami overflow," *Proc. of the 34th Int. Conf. on Coastal Engineering*, Seoul, Korea, doi.org/10.9753/icce.v34.sediment.

Moore, W. and Morgan, C. [1957] "The hydraulic jump at an abrupt drop," *J. Hydraul. Div.* ***83***(6), 1–21.

Ohtsu, I. and Yasuda, Y. [1991] "Transition from supercritical to subcritical flow at an abrupt drop," *J. Hydraul. Res.* **29**(3), 309–328.

Rajaratnam, N. and Ortiz, N. V. [1977] "Hydraulic jumps and waves at abrupt drops," *J. Hydraul. Div.* **103**(HY4), 381–394.

Takegawa, N., Sawada, Y. and Kawabata, T. [2020a] "Geogrid-based countermeasures against scour behind coastal dikes under tsunami overflow," *Mar. Georesour. Geotechnol.* **38**(1), 64–72.

Takegawa, N., Sawada, Y. and Kawabata, T. [2020b] "Scour reduction in sand beds against vertical jets by applying sheet-like countermeasures," *Mar. Georesour. Geotechnol*. doi.org/10.1080/1064119X.2020.1737893.

Tanimoto, R., Tokida, K., Kitagawa, H. and Araki, S. [2012] "Investigation on resistance of earth bank and reduction by dug pool against tsunami," *J. Jpn. Soc. Civ. Eng. Ser. B2* **68**(2), I_316–I_320. (in Japanese)

Tanimoto, R., and Tokida, K. [2012] "Study on structure of dug pool eroded by tsunami flood and its tsunami reduction function," *Int. Symp. Earthq. Eng.* **1**, 143–150.

The OpenFOAM Foundation [2019] "OpenFOAM User Guide version 7,".

Tokida, K., and Tanimoto, R. [2014] "Lessons for countermeasures using earth structures against tsunami obtained in the 2011 Off the Pacific Coast of Tohoku Earthquake," *Soils Found.* **54**(4), 523–543.